*Metallophysics and Advanced Technologies*
*Металофіз. новітні технол.*
*Metallofiz. Noveishie Tekhnol.*
2024, vol. 46, No. 3, pp. 265–277
https://doi.org/10.15407/mfint.46.03.0265
Reprints available directly from the publisher



PACS numbers: 62.20.F-, 68.37.Hk, 68.37.Lp, 81.30.Kf, 81.30.Mh, 81.40.-z, 87.85.jj

# Influence of Thermomechanical and Heat Treatments on the Structure and Mechanical Properties of Biocompatible Ti–(18–20)Nb–(3–4)Zr–(1–1.2)Si Alloys

O. M. Shevchenko, M. M. Kuzmenko, O. Yu. Koval, A. V. Kotko, and S. O. Firstov

*I. M. Frantsevich Institute for Problems in Materials Science, N.A.S. of Ukraine,*
*3 Omelian Pritsak Str.,*
*UA-03142 Kyiv, Ukraine*

The deformed biomedical Ti–(18–20)Nb–(3–4)Zr–(1–1.2)Si (% wt.) alloys are studied. Their rolling is carried out at 950°C by means of the air- and water-cooling; the quenching in water and oil with heating up to 1050°C is also used. As established with the x-ray phase analysis, the hot deformation of Ti–(18–20)Nb–(3–4)Zr–(1–1.2)Si alloys contributes to the β-solid-solution heterogeneity into $\beta_1$ phase based on Ti–Nb and $\beta_2$ phase based on Zr–Ti, as a result of which a final dispersed nonequilibrium ($\alpha'' + \alpha'$) structure is formed after cooling, that reflects the ($\beta_1 + \beta_2$) microstructure formed due to the previous decomposition. After deformation with air cooling, the experimental alloys contain the largest amount of $\alpha'$ phase and have high strength and low plasticity. As shown, a rising of the cooling rate and temperature during quenching leads to the predominance of the orthorhombic $\alpha''$ phase, while the strength of the alloys decreases with a significant increase in plasticity. In the process of deformation and heat treatment, densely and uniformly distributed disperse silicides are also released in the structure, which contribute to the strengthening. For Ti–(18–20)Nb–(3–4)Zr–(1–1.2)Si alloys, the temperature range $T = 1040 \pm 20$°C is established, the quenching from which allows to obtain high mechanical properties: $\sigma_в = 1100$–$1150$ MPa, $\sigma_{0.02} = 800$–$850$ MPa, $\delta = 11$–$11.5\%$. By deformation and quenching of the experimental alloys, a composite material with alloyed soft matrix strengthened by the uniformly distributed dispersed hard particles of silicides is fabricated.

Corresponding author: Olha Mykhailivna Shevchenko
E-mail: omshev@ukr.net

Citation: O. M. Shevchenko, M. M. Kuzmenko, O. Yu. Koval, A. V. Kotko, and S. O. Firstov, Influence of Thermomechanical and Heat Treatments on the Structure and Mechanical Properties of Biocompatible Ti–(18–20)Nb–(3–4)Zr–(1–1.2)Si Alloys, *Metallofiz. Noveishie Tekhnol.*, **46**, No. 3: 265–277 (2024). DOI: 10.15407/mfint.46.03.0265

**Key words:** biocompatible Ti–(18–20)Nb–(3–4)Zr–(1–1.2)Si alloys, deformation, quenching, structure, silicides, mechanical properties.

Досліджено деформовані біомедичні стопи Ti–(18–20)Nb–(3–4)Zr–(1–1,2)Si (% ваг.). Прокатування проводилося за температури у 950°C з охолодженням на повітрі та водою; застосовувалося також гартування у воду та масло з нагрівом до 1050°C. Рентґенофазовою аналізою встановлено, що гаряче деформування стопів Ti–(18–20)Nb–(3–4)Zr–(1–1,2)Si сприяє розшаруванню β-твердого розчину на $\beta_1$-фазу на основі Ti–Nb і $\beta_2$-фазу на основі Zr–Ti, внаслідок чого після охолодження утворюється кінцева дисперсна нерівноважна ($\alpha'' + \alpha'$)-структура, яка відображає мікроструктуру ($\beta_1 + \beta_2$), сформовану через попередній розпад. Після деформації з охолодженням на повітрі дослідні стопи містять найбільшу кількість $\alpha'$-фази та мають високу міцність і низьку пластичність. Показано, що збільшення швидкости охолодження та підвищення температури під час гартування приводить до переважання у них орторомбічної $\alpha''$-фази; водночас міцність стопів понижується зі значним підвищенням пластичности. В процесі деформації та термооброблення в структурі також виділяються щільно й рівномірно розподілені дисперсні силіциди, які вносять свій внесок у зміцнення. Для стопів Ti–(18–20)Nb–(3–4)Zr–(1–1,2)Si встановлено інтервал температур $T = 1040 \pm 20$°C, гартування від якого уможливлює одержати високі механічні властивості: $\sigma_в = 1100–1150$ MPa, $\sigma_{0,02} = 800–850$ MPa, $\delta = 11–11{,}5\%$. Шляхом деформування та гартування дослідних стопів створено композиційний матеріял з леґованою пластичною матрицею, зміцненою рівномірно розподіленими дисперсними твердими частинками силіцидів.

**Ключові слова:** біосумісні стопи Ti–(18–20)Nb–(3–4)Zr–(1–1,2)Si, деформація, гартування, структура, силіциди, механічні властивості.

*(Received 31 October 2023; in revised form, 10 December 2023)*

## 1. INTRODUCTION

The development of new titanium alloys for implantology continues in the direction of excluding from their composition some elements harmful to the human body, as well as strengthening their osteointegration and mechanical properties [1, 2]. Recently, titanium alloys alloyed with biocompatible β stabilizing elements, in particular niobium [3], have been developed, which have a lower modulus of elasticity, closer to the modulus of elasticity of bone.

Biomedical alloys based on the Ti–Nb system, additionally doped with silicon for better osteointegration, were also proposed [4–8]. It was established that alloys with 18–20% wt. niobium and a hypereutectoid silicon content of 1–1.2% wt. exhibit higher mechanical properties and biocompatibility in the Ti–Nb–Si system. The deformation modes of Ti–(18–20)Nb–(1–1.2)Si alloys were developed and the opti-

mal temperature at which quenching of the deformed alloys allows obtaining high mechanical characteristics was determined [9].

The properties of alloys of the Ti–Nb and Ti–Nb–Si systems can be further improved by alloying with biocompatible zirconium [10–13]. In Ti–Nb–Zr [10] and Ti–Nb–Zr–Si [12, 13] alloys, zirconium has an additional β stabilizing effect, which grows with an increase in the content of other β stabilizers (Nb and Si). Zirconium reduces the solubility of silicon and increases the release of silicides in alloys of the Ti–Nb–Zr–Si system, due to which the alloys are strengthened [12, 13]. The aim of this work is to optimize the technology of deformation and heat treatment of Ti–(18–20)Nb–(3–4)Zr–(1–1.2)Si (% wt.) alloys.

## 2. RESEARCH MATERIALS AND METHODS

Experimental Ti–(18–20)Nb–(3–4)Zr–(1–1.2)Si alloys were obtained by electron beam melting [14]. The following charge materials were used: ВТ1-0 titanium, НбШ-1 niobium, ктц-110 zirconium, КР-00 silicon. The used smelting method ensured the formation of ingots of the Ti–Nb–Zr–Si system alloys with a diameter of 60 mm and a length of 640–650 mm, which are quite homogeneous in structure and chemical composition.

Hot deformation of ingots was carried out at a temperature of 950°C by screwing rolling up to ∅ 12 mm with air or water cooling. The obtained rods were cut into samples, which were quenched in oil and water with a holding time of 30 min at 1050°C. After deformation and heat treatment, tensile tests of the mechanical properties were performed.

The structure was studied by optical (Jenaphot-2000), electron scanning (Proton-21, Superprobe-733) and transmission (JEOL JEM 100X) microscopy. The x-ray phase diffraction analysis was carried out on a DRON-3M diffractometer in monochromatic Cu$K_\alpha$-radiation, at an accelerating voltage of 40 kV and a current of 25 mA, in the angular range $2\Theta = 30–90°$ with a step of 0.05° and with a stop of 5 s/step. The results were processed in PowderCell software.

## 3. RESULTS AND DISCUSSION

The properties of alloys after deformation and heat treatment are influenced by the phase composition, the ratio and size of the structural components. When the cast alloys of the Ti–Nb–Zr–Si system are heated, the non-equilibrium phases disintegrate with the redistribution of silicon and the release of silicides. The largest amount of silicides was observed on the quenching of these alloys from low temperatures of 900–1000°C, close to the eutectoid transformation (865°C in the Ti–Si system) [6, 7, 13]. Figure 1 shows the structure of the cast

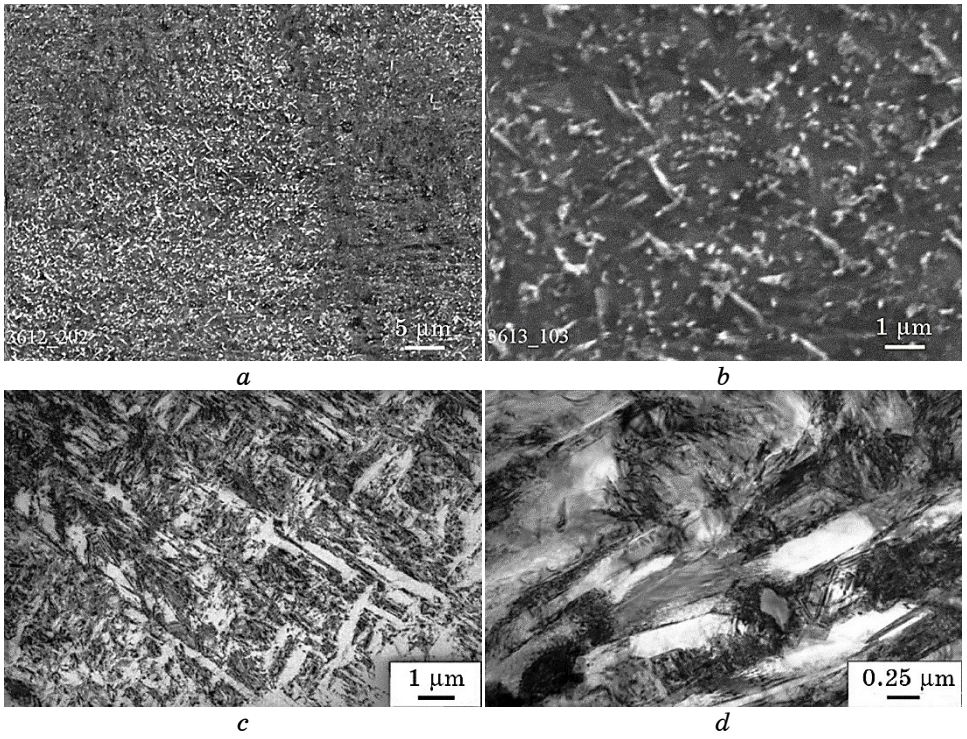


**Fig. 1.** Electron microscopy of the cast Ti–18Nb–4Zr–1Si alloy quenched from 900°C with a holding time of 5 min: scanning (*a*, *b*), transmission (*c*, *d*).

alloy Ti–18Nb–4Zr–1Si quenched from 900°C with holding for 5 minutes, where densely distributed silicide precipitates are clearly visible. At the same time, almost all silicon binds with zirconium and titanium to form silicides $(Ti,Zr)_3Si$, ≤ 0.2% Si remains in the solid solution of the cast Ti–8Nb–4Zr–1Si alloy [11], that leads to a significant decrease in hardness. When the alloy is heated to higher temperatures ≥ 1100°C, the silicides begin to dissolve.

Rolling of the cast Ti–(18–20)Nb–(3–4)Zr–(1–1.2)Si alloys occurred in β area at a temperature of ≅ 950°C with different cooling speeds: in air and water. After the deformation with air cooling, quenching was also applied.

In order to determine the optimal mode of heat treatment of the deformed Ti–(18–20)Nb–(3–4)Zr–(1–1.2)Si alloys, the quenching in water was carried out at the temperature range of 1000–1100°C in an interval of 20°. The dependences of $\sigma_в$, $\sigma_{0.02}$, δ on the quenching temperature are shown in Fig. 2. Dashed lines show mechanical properties of the experimental alloys for tension in the deformed state as initial values. The arrows show changes in the level of $\sigma_в$, $\sigma_{0.02}$, δ after quenching,

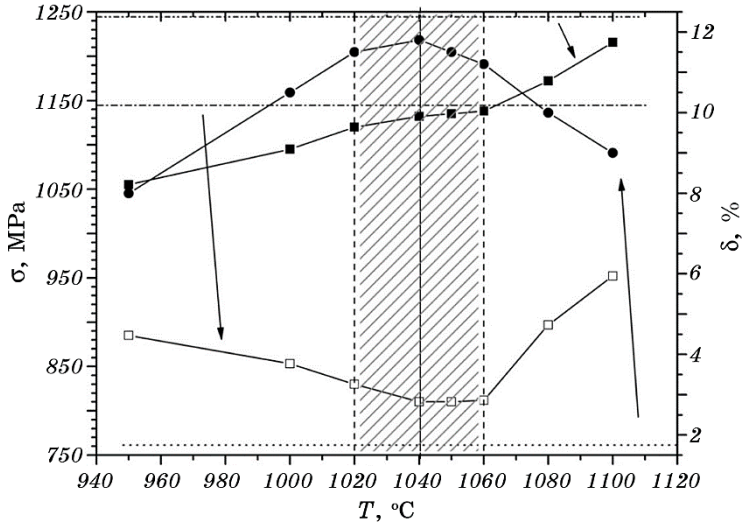


**Fig. 2.** The tensile mechanical properties of deformed Ti–(18–20)Nb–(3–4)Zr–(1–1.2)Si alloys after quenching in water: $\sigma_в$ (■), $\sigma_{0.2}$ (□), $\delta$ (•).

and the range of quenching temperatures that provide the optimal set of mechanical properties is also highlighted.

For the deformed Ti–(18–20)Nb–(3–4)Zr–(1–1.2)Si alloys, a temperature range of $T = 1040 \pm 20$°C has been established, the quenching from which allows obtaining almost identical high mechanical characteristics: $\sigma_в = 1100–1150$ MPa, $\sigma_{0.02} = 800–850$ MPa, $\delta = 11–11.5\%$. Decreasing of the yield strength $\sigma_{0.02}$ after quenching from temperatures < 1060°C can be explained by more decomposition of the solid solution with forming the great amount of silicides, and as a result the presence of poor with β stabilizers, unstable β phase which undergoes deformation martensitic transformation in tension. Quenching at 1040–1060°C probably fixes the maximum quantity of metastable β phase, while the difference between the temporary fracture resistance $\sigma_в$ and the yield strength $\sigma_{0.02}$ is > 300 MPa. At higher quenching temperatures, almost the entire β phase undergoes transformation and the amount of martensite increases, at the same time silicides are dispersed due to partial dissolution [13], the consequence of which is an increase in $\sigma_в$, $\sigma_{0.02}$ with a simultaneous decrease in plasticity $\delta$ (Fig. 2).

According to x-ray phase analysis the deformed and quenched Ti–(18–20)Nb–(3–4)Zr–(1–1.2)Si alloys contain α′ and α″ phases with their different ratio, residual β phase, and silicides (Fig. 3, Table 1). It should be noted that a sharp peak located at angles $2\theta \cong 50–51°$ (Fig. 3) is observed on the XRD-patterns, which cannot be attributed to the existing β, α″, α′ phases. Considering its rather significant intensity, the appearance of such a peak cannot be explained either by the presence of

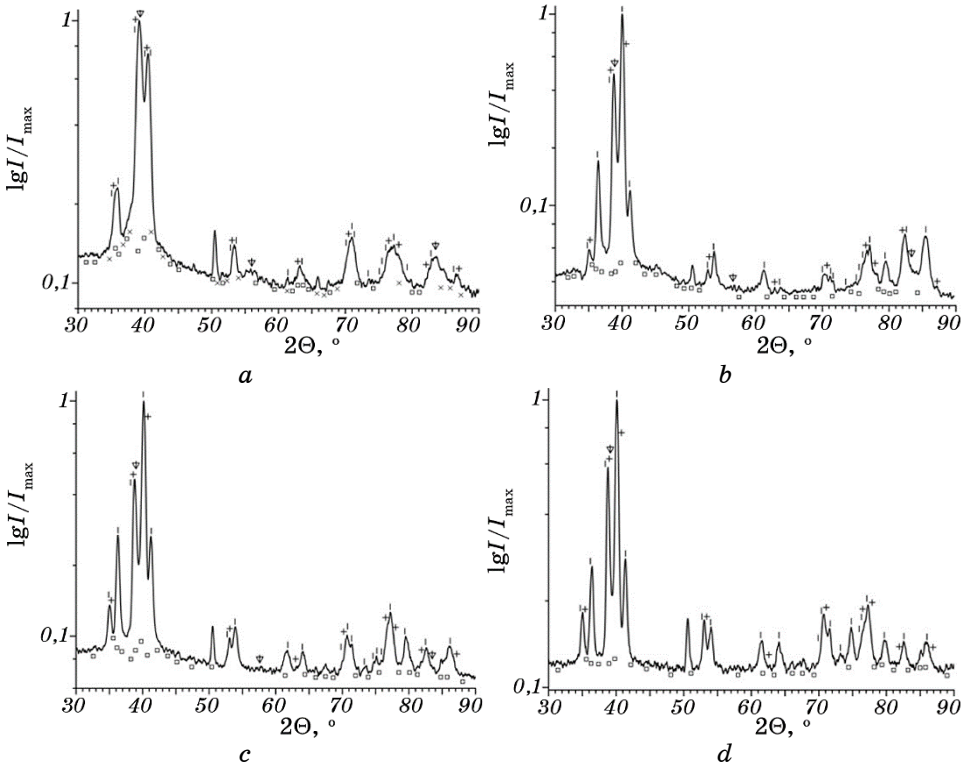


**Fig. 3.** XRD-patterns of Ti–(18–20)Nb–(3–4)Zr–(1–1.2)Si alloy: after the screwing rolling at 950°C with cooling in air (*a*) and water (*b*), after the quenching in oil (*c*) and water (*d*) at 1050°C, 30 minutes: α′ phase (+), α″ phase (|), β phase (↓), $Ti_3Si$ (□), $Ti_5Si_3$ (×).

silicides or by the presence of the ω phase. In cast Ti–18Nb–*x*Zr–1Si alloys [12], the same Bragg reflection in the diffraction pattern to the left of the main $(200)_\beta$ reflex appeared only when the zirconium content reached 8% wt., which indicates the formation of another β phase with a lattice parameter $a \cong 3.615–3.595$ Å based on a Zr–Ti solid solution.

The appearance of another phase with a higher parameter of b.c.c. lattice, but lower intensity compared to the reflection of the main β phase, was previously observed in cast Ti–Nb β alloys [15] with a high niobium content of 37.5 and 45% wt. One of the possible mechanisms for the formation of a double b.c.c. phase is considered the segregation of elements because of dendritic liquation during crystallization due to the difference in the melting temperatures of the components since the content of alloying elements in the axes of dendrites and interdendritic areas can differ significantly. But, in the as-cast state of the experimental Ti–(18–20)Nb–(3–4)Zr–(1–1.2)Si (α + β) alloys of the martensit-

**TABLE 1.** Phase composition of Ti–(18–20)Nb–(1–1.2)Si alloys: after the screwing rolling at 950°C with cooling in air (1) and water (2); after the quenching in oil (3) and water (4) at 1050°C, 30 min.

| | α (α′) | | | α″ | | | | β | | $(Ti,Zr)_3Si$/ $(Ti,Zr)_5Si_3$, % mass |
|---|---|---|---|---|---|---|---|---|---|---|
| | *a* | *c* | % mass | *a* | *b* | *c* | % mass | *a*, Å | % mass | |
| | Å | | | Å | | | | | | |
| 1 | 2.9785 | 4.6537 | 43 | 3.0804 | 5.0930 | 4.6895 | 49.4 | 3.2674 | 2.8 | 2.8/1.9 |
| 2 | 2.9620 | 4.6577 | 32.2 | 3.0258 | 4.9720 | 4.6613 | 60.1 | 3.2866 | 2.6 | 5.0/0 |
| 3 | 2.9625 | 4.6578 | 16.4 | 3.0107 | 4.9713 | 4.6594 | 75.8 | 3.2686 | 2.3 | 5.5/0 |
| 4 | 2.9639 | 4.6579 | 16.1 | 3.0229 | 4.9654 | 4.6657 | 74.4 | 3.2757 | 3.3 | 5.8/0.3 |

ic class, dendritic liquation was quite weak [13], the structure after crystallization consisted mainly of the α″ phase, the β phase had no signs of delamination and its content reached ≅ 12% .

The second mechanism of the appearance of a double β phase is the spinodal decomposition of a solid solution. Phase separation is facilitated by the difference in atomic radii, especially the presence in alloys of elements with small atomic sizes: hydrogen [15], oxygen [16], or silicon in alloys of the Ti–Nb–Zr–Si system, which creates conditions for the formation of clusters. Thus, during heat treatment of Ti–Nb–O alloys [16] in the β phase, nanodomains of Nb-poor and Ti, O enriched $\beta_1$, as well as Nb-enriched, but Ti and O depleted $\beta_2$ are formed, which leads to the nanoscale ($\beta_1 + \beta_2$) spinodal microstructure. In the cast Ti–Zr–Ta β alloys [17], a nanostructure corresponding to the spinodal decomposition of the original β phase was also formed: semi-coherent particles of the $\beta_2$ phase with an increased Ta content interspersed in the Zr-enriched $\beta_1$ matrix with strain accommodation due to edge dislocations at the phase boundary and modulation along the elastic-soft directions <100> in b.c.c. lattice. Such a structure affects strengthening, which is associated with a barrier to the movement of dislocations in the form of inclusion boundaries. Unlike traditional decay, spinodal decomposition does not require the nucleation of particles and allows obtaining uniform nanostructures without long-term ageing.

On rolling in the β area of Ti–(18–20)Nb–(3–4)Zr–(1–1.2)Si alloys, the deformation can stimulate the spinodal decomposition of the β solid solution. In metals with cubic lattices, {100} <110> deformation texture is formed, so the $\beta_2$ phase in the experimental alloys has the corresponding predominant orientation, which is observed in the form of an increased intensity of its (200) line in the diffraction pattern (Fig. 3). It is likely that upon further cooling the $\beta_1$ phase transforms into α″ phase, $\beta_2$ into α′, with remnants of the corresponding β phases between the martensitic plates, and the final dispersed structure (α″ + α′) reflects the mi-

crostructure ($\beta_1 + \beta_2$) formed through spinodal decomposition.

During deformation processing with air-cooling of Ti–(18–20)Nb–(3–4)Zr–(1–1.2)Si alloys, the cooling rate is higher at high temperatures, where the martensitic transformation $\beta \rightarrow \alpha'$ occurs. As a result, a thin needle-like $\alpha'$ phase is formed (Fig. 4, *a*, *b*), which has a significant distortion of the crystal lattice $c/a = 1.562$ (for $\alpha$ Ti $c/a = 1.587$). Upon further cooling, a dispersed $\alpha''$ phase as separate areas between the primary needles appears, the orthorhombicity of which is close to unity $b(3)^{-1/2}/a = 0.955$ that indicates its lower doping with $\beta$ stabilizers. At the same time, the diffraction pattern does not show the splitting of the lines, but only their broadening (Fig. 3, *a*). In the structure of deformed Ti–(18–20)Nb–(3–4)Zr–(1–1.2)Si alloys cooled in air, there is also a small amount of primary $(Ti,Zr)_5Si_3$ silicides (Table 1), which were formed in the cast state after crystallization, and secondary

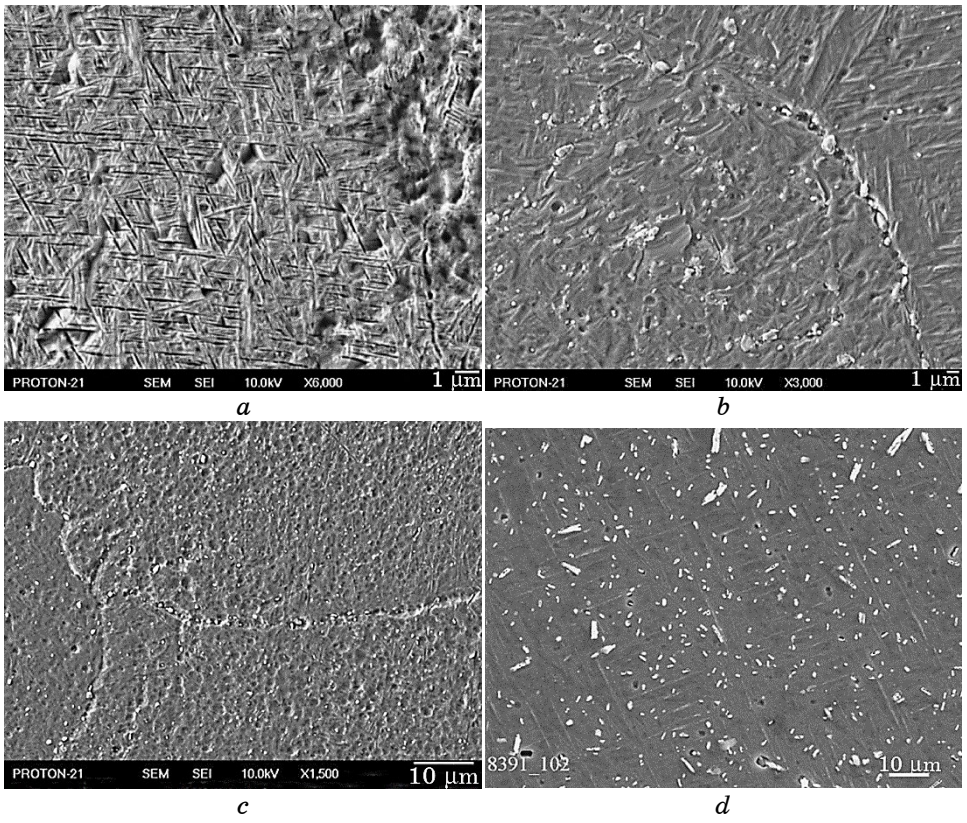


*a* *b* *c* *d*

**Fig. 4.** Scanning electron microscopy of Ti–(18–20)Nb–(3–4)Zr–(1–1.2)Si alloys: deformation at 950°C with air cooling (*a*), deformation at 950°C with cooling by water (*b*), quenching of the deformed alloy into oil at $T = 1050$°C, 30 minutes (*c*), quenching of the deformed alloy in water at $T = 1050$°C, 30 minutes (*d*).

**TABLE 2.** Mechanical properties of Ti–(18–20)Nb–(3–4)Zr–(1–1.2)Si alloys after different hot deformation and heat treatment modes.

| | Treatment | Mechanical tensile properties | | |
|---|---|---|---|---|
| | | $\sigma_{0.2}$, MPa | $\sigma_в$, MPa | $\delta$, % |
| 1 | Rolling at 950°C, air cooling | 1145 | 1250 | 1,7 |
| 2 | Rolling at 950°C, water cooling | 885 | 1055 | 8 |
| 3 | 1 + quenching at 1050°C, 30 minutes in oil | 760 | 1025 | 12 |
| 4 | 1 + quenching at 1050°C, 30 minutes in water | 810 | 1135 | 11,5 |

$(Ti,Zr)_3Si$ silicides, which were released during cooling due to the peritectoid transformation at 1170°C: $\beta + (Ti,Zr)_5Si_3 \rightarrow (Ti,Zr)_3Si$ [13]. The formation of such a non-equilibrium deformed structure causes high strength $\sigma_в \cong 1250$ MPa and low plasticity $\delta < 2\%$ (Table 2).

An increase in the cooling rate and an increase in temperature during quenching of deformed Ti–(18–20)Nb–(3–4)Zr–(1–1.2)Si alloys leads to the formation of a larger amount of orthorhombic $\alpha''$ phase (Table 1), which has a dispersed lenticular thin-lamella structure (Fig. 4, *b*, *d*). This also results in a decrease in the values of orthorhombicity of $\alpha''$ martensite $b(3)^{-1/2}/a = 0.953–0.948$ and the splitting of its lines on the XRD patterns (Fig. 3, *b*–*d*), due to a greater saturation with alloying elements. Accordingly, the amount of the $\alpha'$ phase decreases, and its $c/a = 1.572$ (Table 1) increases, which means a decrease in doping of this phase. The strength of deformed Ti–(18–20)Nb–(3–4)Zr–(1–1.2)Si alloys after quenching decreases compared to air-cooling with a significant increase in plasticity due to the predominant amount of the $\alpha''$ phase (Table 2).

In the quenching process, an additional separation of tertiary silicides $(Ti,Zr)_3Si$ occurs because of the eutectoid transformation: $\beta \rightarrow \alpha'' + (Ti,Zr)_3Si$. Thus, Ti–(18–20)Nb–(3–4)Zr–(1–1.2)Si alloys after deformation and heat treatment contain densely and uniformly distributed silicide particles (Fig. 4) with a total amount of $\cong 5–6\%$ mass (Table 1). The most intense lines of silicides on the diffractograms practically coincide with the lines of the main phases, so their presence is evidenced by an increase in the background near the main lines and the higher total intensity (Fig. 3). Electron-microscopy study showed a large number of both coarse and dispersed silicides in the quenched alloys between small, differently oriented, acicular and lenticular martensitic plates (Fig. 5).

Eutectoid silicides are released during the quenching process both in the form of highly dispersed particles between the plates of the $\alpha''$ phase, and on the already existing secondary $(Ti,Zr)_3Si$ silicides, which

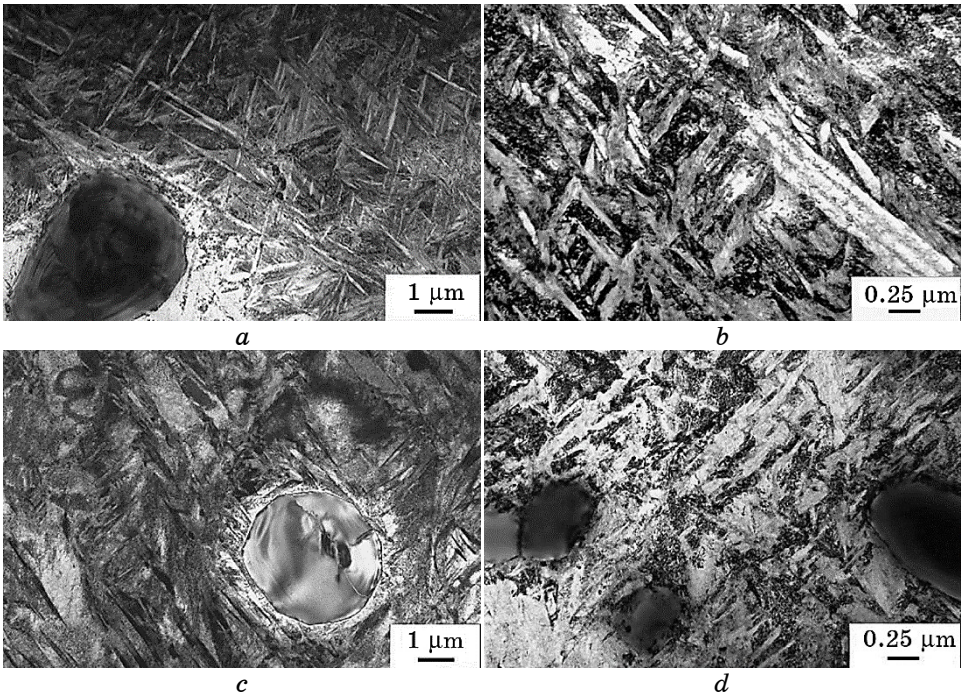


**Fig. 5.** Transmission electron microscopy of Ti–(18–20)Nb–(3–4)Zr–(1–1.2)Si alloy: after the screw rolling at 950°C with water cooling (*a*, *b*), after the deformation with the additional quenching in water at 1050°C (*c*, *d*).

results in their growth. The formation of dispersed silicides on the surfaces of martensitic plates and in β layers occurs due to deformation and heat treatment of the experimental alloys. This leads to their grid-like distribution, which is a resistance to the movement of dislocations and provides additional strengthening.

Tensile failure of the alloy, deformed with air cooling, is brittle-viscous, and pitted, with the presence of spalled facets in areas of the lamellar α′ phase (Fig. 6, *a*). Low-energy dimples dominate the fracture surface after quenching at a lower temperature of 950°C (Fig. 6, *b*). The fracture of the alloy quenched at 1050°C is viscous, high-energy, with small pits (Fig. 6, *c*). In a softer matrix, the deformation pits are formed, at the bottom of which silicides remain (Fig. 6, *d*).

Both the level of the phases alloying (solid-solution hardening) and the amount and size of silicides (dispersion hardening) affect the mechanical properties. In the solid solution of Ti–(18–20)Nb–(3–4)Zr–(1–1.2)Si alloys, ≤ 0.2% Si remains according to calculations [13], and the α′ phase contains more dissolved silicon, and, accordingly, less silicides than the α″ phase. The fracture mechanism of Ti–(18–20)Nb–(3–

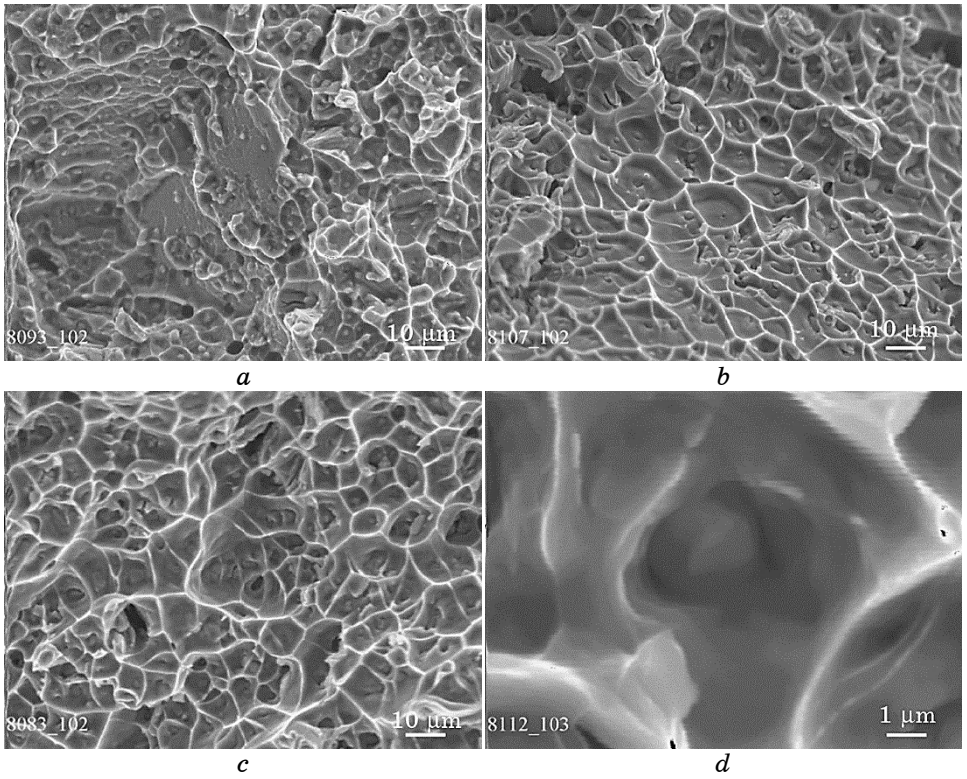


**Fig. 6.** The fracture surface of the Ti–(18–20)Nb–(3–4)Zr–(1–1.2)Si alloy: deformed at 950°C, cooled in air (*a*), deformed at 950°C with cooling by water (*b*), quenched at 1050°C, 30 minutes in water (*c*, *d*).

4)Zr–(1–1.2)Si alloys shows that deformation and quenching create a composite material with an alloyed plastic matrix, which is strengthened by uniformly distributed, dispersed solid particles of silicides.

## 4. CONCLUSIONS

After the hot deformation at 950°C with air-cooling of Ti–(18–20)Nb–(3–4)Zr–(1–1.2)Si alloys, approximately the same amount of $\alpha'$ and $\alpha''$ phases was formed. Such a non-equilibrium structure has high strength $\sigma_в \cong 1250$ MPa and low plasticity $\delta < 2\%$. Quenching of Ti–(18–20)Nb–(3–4)Zr–(1–1.2)Si alloys leads to the predominance of the orthorhombic $\alpha''$ phase in their structure, correspondingly, the strength decreases with a significant increase in plasticity. The temperature range $T = 1040 \pm 20$°C was established, from which quenching of deformed alloys Ti–(18–20)Nb–(3–4)Zr–(1–1.2)Si allows obtaining

an optimal complex of high mechanical properties: $\sigma_в = 1100–1150$ MPa, $\sigma_{0.02} = 800–850$ MPa, $\delta = 11–11.5\%$.

The structure of Ti–(18–20)Nb–(3–4)Zr–(1–1.2)Si alloys after deformation and heat treatment also contains dispersed silicides densely and uniformly distributed between small martensite plates. The formation of a large amount of silicides ($\cong 5–6\%$ mass) decreases the silicon content in the solid solution and reduces its strength. However, at the same time, the mesh-like distribution of silicides formed due to deformation and heat treatment is a resistance to the movement of dislocations and provides dispersion hardening. In this way, a composite material with an alloyed soft matrix and uniformly distributed hard silicide particles was created.

In the deformed and quenched Ti–(18–20)Nb–(3–4)Zr–(1–1.2)Si alloys, x-ray structural analysis showed that, in addition to $\alpha'$, $\alpha''$, residual $\beta$ phase and silicides, a peak was also observed indicating the presence of another $\beta$ phase based on a Zr–Ti solid solution with a lattice parameter $a \cong 3.615–3.595$ Å. The appearance of this phase can be explained by the spinodal decomposition of the $\beta$ solid solution, which is stimulated by the stresses during deformation. This is facilitated by the difference in the atomic sizes of the components, in particular the presence in alloys of silicon and zirconium and the possible formation of clusters. The delamination of the $\beta$ phase during deformation probably affects the formation of the final dispersed $(\alpha'' + \alpha')$-structure, and provides high mechanical properties.

## REFERENCES

1. Y. Okazaki, S. Rao, T. Tateishi, and Y. Ito, *Mater. Sci. Eng. A*, **243**, Nos. 1–2: 250 (1998).
2. M. Niinomi, *Mater. Sci. Eng. A*, **243**, Nos. 1–2: 231 (1998).
3. Y. Zhang, D. Sun, J. Cheng, J. K. H. Tsoi, and J. Chen, *Regen. Biomater.*, **7**, No. 1: 119 (2020).
4. O. M. Shevchenko, L. D. Kulak, M. M. Kuzmenko, and S. O. Firstov, *Metallofiz. Noveishie Tekhnol.*, **41**, No. 3: 363 (2019) (in Ukrainian).
5. O. M. Shevchenko, L. D. Kulak, M. M. Kuzmenko, A. V. Kotko, and S. O. Firstov, *Metallofiz. Noveishie Tekhnol.*, **39**, No. 6: 823 (2017) (in Ukrainian).
6. O. M. Shevchenko, L. D. Kulak, M. M. Kuzmenko, and S. O. Firstov, *Mater. Sci.*, **55**, No. 4: 577 (2020).
7. O. M. Shevchenko, L. D. Kulak, M. M. Kuzmenko, O. Yu. Koval, A. V. Kotko, N. V. Ulyanchich, O. O. Piven, T. P. Ruban, and S. O. Firstov, *Metallofiz. Noveishie Tekhnol.*, **43**, No. 7: 887 (2021) (in Ukrainian).
8. O. M. Shevchenko, L. D. Kulak, M. M. Kuzmenko, O. Yu. Koval, and S. O. Firstov, *Metallofiz. Noveishie Tekhnol.*, **44**, No. 8: 1059 (2022) (in Ukrainian).
9. O. M. Shevchenko, L. D. Kulak, M. M. Kuzmenko, O. Yu. Koval, and

S. O. Firstov, *Metallofiz. Noveishie Tekhnol.*, **45**, No. 3: 329 (2023) (in Ukrainian).
10. M. Abdel-Hady, H. Fuwa, K. Hinoshita, H. Kimura, Y. Shinzato, and M. Morinaga, *Scripta Mater.*, **57**, No. 11: 1000 (2007).
11. Q. Li, M. Niinomib, M. Nakaib, Zh. Cuia, Sh. Zhua, and X. Yang, *Mater. Sci. Eng. A*, **536**: 197 (2012).
12. O. M. Shevchenko, L. D. Kulak, M. M. Kuzmenko, and S. O. Firstov, *Metallofiz. Noveishie Tekhnol.*, **42**, No. 2: 237 (2020) (in Ukrainian).
13. O. M. Shevchenko, L. D. Kulak, M. M. Kuzmenko, A. V. Kotko, and S. O. Firstov, *Mater. Sci.*, **58**, No. 2: 180 (2022).
14. N. I. Grechanyuk, L. D. Kulak, N. N. Kuzmenko, Yu. O. Smashnyuk, A. V. Demchishin, and A. E. Fisk, *Electrometallurgy Today*, No. 2: 17 (2017) (in Russian).
15. A. Thoemmes, I. A. Bataev, D. V. Lazurenko, A. A. Ruktuev, I. V. Ivanov, C. R. M. Afonso, A. Stark, and A. M. Jorge Jr., *Mater. Sci. Eng. A*, **818**: 141378 (2021).
16. Y. Ishiguro, Y. Tsukada, and T. Koyama, *Computational Mater. Sci.*, **151**: 222 (2018).
17. A. Biesiekierski, D. Ping, Y. Li, J. Lin, K. S. Munir, Y. Yamabe-Mitarai, and C. Wen, *Acta Biomater.*, **53**: 549 (2017).